New Insights into the Physicochemical and Electrochemical Characterization of Gold Phthalocyanine-Based Materials

Wend-Kuny Guy Aristide Nitiema, Bertrand Ouemega, Marie-Agnès Lacour, Sarra Knani, Eddy Petit, Valerie Flaud, Nathalie Masquelez, David Cornu, Mabinty Bayo-Bangoura, Yaovi Holade

Journal of The
Electrochemical Society

New Insights into the Physicochemical and Electrochemical Characterization of Gold Phthalocyanine-Based Materials

To cite this article: Wend-Kuny Guy Aristide Nitiema *et al* 2023 *J. Electrochem. Soc.* **170** 106508

Journal of The Electrochemical Society, 2023 **170** 106508

New Insights into the Physicochemical and Electrochemical Characterization of Gold Phthalocyanine-Based Materials

Wend-Kuny Guy Aristide Nitiema,[1,2] Bertrand Ouemega,[1] Marie-Agnès Lacour,[3] Sarra Knani,[2] Eddy Petit,[2] Valerie Flaud,[4] Nathalie Masquelez,[2] David Cornu,[2] Mabinty Bayo-Bangoura,[1,z] and Yaovi Holade[1,*,z]

[1]*Laboratoire de Chimie Moléculaire et de Matériaux, Université Joseph Ki-Zerbo, Ouagadougou, 03 BP 7021, Ouagadougou, Burkina Faso*
[2]*Institut Européen des Membranes, IEM, UMR 5635, Univ Montpellier, ENSCM, CNRS, 34090 Montpellier, France*
[3]*ChemLab, ENSCM, 34296 Montpellier, France*
[4]*Institut Charles Gerhardt Montpellier, ICGM, UMR 5253, Univ Montpellier, ENSCM, CNRS, 34090 Montpellier, France*

Gold phthalocyanine-based materials can allow to combine the unique physical properties of the metallophthalocyanine with gold for numerous applications such as (photo)-electrochemistry or the so-called single atom catalysts (SACs), which require very small amounts of metal. However, there is currently a lack of physico-chemical and electrochemical knowledge to consider such applications. We report the synthesis and the physical characterization of three types of materials, the unsubstituted and the octo-substituted gold phthalocyanines AuPc, $AuPc(CN)_8$ and $AuPc(COOH)_8$, which were successfully synthesized. To interrogate the physicochemical and electrochemical properties of the as-synthesized materials, we have performed a multi-variant study by integrating different methods (UV–vis, FTIRS, TGA-TDA, HR-ESI-MS, SEM-EDX, XRD, XPS, CV). UV–vis confirms the shift towards high wavelengths (bathochromic effect) for the transition Q-band (charge transfer from pyrrolic carbons to neighboring atoms in the macrocycle) of $AuPc(CN)_8$ and $AuPc(COOH)_8$ compared to AuPc. CV in both aqueous and non-aqueous provides the first electrochemical insights into the phthalocyanine ring reduction and oxidation, $AuPc/[AuPc]^-$, $[AuPc]^-/[AuPc]^{2-}$ and $[AuPc]^{2-}/[AuPc]^{3-}$. The results delineate a possible rational pathway for AuPc-based materials or alternatively, their transformation into SACs, where a single Au atom is embedded in a nanostructured carbon-nitrogen scaffold.
 [DOI: 10.1149/1945-7111/ad032b]

Manuscript submitted April 21, 2023; revised manuscript received October 11, 2023. Published October 26, 2023.

Supplementary material for this article is available online

Metallophthalocyanines (MPc) have unique physicochemical properties (optical, electrical, etc.) that make them functional objects for many applications (catalysis, pigments, dyes, digital data storage, photodynamic therapy, etc.).[1–9] For example, phthalocyanines absorb strongly in the visible spectrum (λ = 400–800 nm) and are therefore well suited for optical and spectroelectrochemical applications.[1,3,10–12] Kotiaho et al.[13] have spectroscopically studied the photoinduced processes in phthalocyanine-functionalized gold nanoparticles (Pc-AuNPs) and found a slower relaxation compared to AuNPs, confirming the energy transfer from the photoexcited phthalocyanine to gold. The properties of MPc-based materials can be elegantly tuned by changing the central metal and/or making the peripheral substitution,[1–4,13,14] which also allows to increase the solubility of MPc complexes.[3,15–17] Specifically, various MPc (M = Co, Fe, Ni, Zn, etc.)[10] have been widely studied in electrochemistry as molecular materials or as the basis for single atom metal catalyst (SACs) due to $M-N_4-C$ centers.[5,14,18] For example, a Fe and Zn-containing nitrogen-doped carbon framework after co-pyrolysis of FePc and ZnPc results in a half-wave potential ($E_{1/2}$) of 0.9 V_{RHE} in 0.1 M KOH (up to 53 mV superior to Pt/C), a 4-electron transfer oxygen reduction reaction (ORR), and fair electrochemical stability.[19]

AuPc-based materials have received little attention, however, the mononuclear Au(+II) has a potential in catalysis and medicinal chemistry.[1,20–25] In 1995, MacCragh and Koski have reported the first synthesis of monocular AuPc (Scheme 1, without axial ligand X) with ultraviolet–visible (UV–vis) absorption peaks at 662, 633, 601, and 348 nm.[24] This "putative AuPc"[1] would lead to Au(+II) with d^9 electron configuration (usual oxidation states being 0 ($d^{10}s^1$), +I (d^{10}) and +III (d^8)). In 2012, Wong et al.[1] reported a failure to reproduce the reported synthesis of AuPc, reigniting the discussion about the possibility of obtaining such a material composed of paramagnetic gold(II) species. Recently, Katja Heinze's team used a porphyrin strategy to obtain gold(II) complex material.[21] To our knowledge, there is almost no use of X-ray photoelectron spectroscopy (XPS), scanning electron microscopy (SEM) and energy dispersive X-ray spectroscopy (EDX) to study the oxidation state of the different elements, the morphology and the composition. Also, no electrochemical studies of AuPc-based materials have been reported, however, they could catalyze a number of electrocatalytic reactions.[18] The mastery of a method for the synthesis of AuPc-based materials and the knowledge of their electrochemistry could make it possible to develop single atom catalysts (SACs).[14,18,26] In fact, out of 210 SACs models for the on-site O_2-to-H_2O_2 electroconversion, density functional theory (DFT) calculations suggest that among 149 thermodynamically and electrochemically stable SACs, Au-N_4-C (see Scheme 1) derived from AuPc-based materials would be a candidate if experimentally synthesized.[18] Hence, before exploring AuPc-based materials for SACs, which have the unique advantage of requiring only small amount of the noble metal, it is essential to master a replicable synthesis methodology, and to know the detailed physico-chemistry and electrochemistry of the parent materials. Herein, we report the extensive physicochemical and electrochemical study of three types of gold phthalocyanines, namely AuPc (unsubstituted), $AuPc(CN)_8$ (octo-substituted CN groups) and $AuPc(COOH)_8$ (octo-substituted COOH groups), see Scheme 1. We decided to use "AuPc" generically because we were uncertain about the presence or absence of Cl (Scheme 1), i.e. our results did not allow to definitively assert the formation of a gold (II) phthalocyanine. This does not undermine the potential of our results as a solid baseline for future works by revealing new structural and electrochemical insights.

*Electrochemical Society Member.
[z]E-mail: mabinty.bayo@ujkz.bf; yaovi.holade@enscm.fr

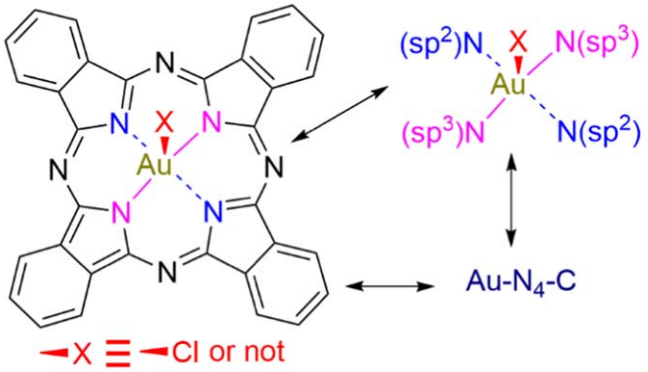

Scheme 1. Gold phthalocyanine: Putative AuPc is the absence of the axial ligand X.

Experimental

Chemicals and materials.—Hydrogen tetrachloroaurate (III) trihydrate [$HAuCl_4{\cdot}3H_2O$, ACS, 99.99% (metals basis), Au 49.0% min, Alfa Aesar], nitrobenzene (Sigma Aldrich), 1,2-dicyanobenzene (phthalonitrile, Alfa Aesar), 1,2,4,5-tetracyanobenzene [>98.0%(HPLC)(N), TCI Chemicals], toluene (Alfa Aesar), methanol (Alfa Aesar), tetra-n-butylammonium hexafluorophosphate ([^{n}Bu_4N][PF_6], 98%, Across Organics), acetone (Alfa Aesar), molecular sieve 3 Å (VWR), Nafion suspension (5 wt%, Sigma Aldrich), sodium hydroxide (NaOH, ⩾98%, Sigma Aldrich), hydrochloric acid (HCl, 37%, Sigma Aldrich), ethylenediaminetetraacetic acid (EDTA, (>98.5%, Sigma Aldrich), filtration membrane (0.2 μm, Whatman), dimethylsulfoxide (DMSO, HPLC grade, 99.9+%, ThermoFisher Scientific), dimethylformamide (DMF, 99%, ThermoFisher Scientific), and sulfuric acid (H_2SO_4, 97%, Honeywell) were used as received. Ar (grade 5.0) was purchased from Air Liquide (France). Ultrapure water was produced from a Millipore Milli-Q source (MQ, 18.2 MΩ cm at 20 °C).

Preparation of AuPc, AuPc(CN)$_8$ and AuPc(COOH)$_8$.— *AuPc synthesis.*—Typically, in a 250 ml monocol flask, tetrachloroaurate trihydrate acid (506 mg, 1.28×10^{-3} mol), phthalonitrile (660 mg, 5.15×10^{-3} mol) and nitrobenzene (5 ml) were introduced. The mixture was refluxed (∼225 °C) for 20 min. Initially yellow, the reaction medium turns brick red, then green. After cooling to room temperature, the product was precipitated in acetone and filtered through a Buchner system before drying in an oven (40 °C, overnight). Next, the product was successively (filtration between two steps) treated by NaOH (10%, refluxed, 15 min), HCl (10%, refluxed, 15 min) and EDTA (10 mM, stirred, RT, 30 min) before a Soxhlet step with toluene (48 h) and acetone (48 h). The yield was 37%.

Preparation of AuPc(CN)$_8$.—In a typically synthesis, 1,2,4,5-tetracyanobenzene (1.45 g, 8.12×10^{-3} mol) and tetrachloroaurate trihydrate acid (0.8 g, 2.03×10^{-3} mol) were mixed in a 250 ml monocol flask containing nitrobenzene (5 ml). The reaction mixture was refluxed (∼225 °C, 20 min). After 15 min of heating, the initially yellow colored reaction medium turns green. During the reaction, the coloration intensifies and a precipitate appears. After cooling to room temperature, the product was filtered on a Buchner system and washed with ethanol before being dried in an oven (40 °C, overnight). The crude product was then Soxhlet purified successively with toluene, methanol and ethanol for 48 h per solvent. The yield was 86%.

Preparation of AuPc(COOH)$_8$.—In a 100 ml monocol flask containing 20 ml of HCl (4 M, 8×10^{-2} mol), $AuPc(CN)_8$ (0.896 g, 9.85×10^{-4} mol) from the above synthesis was introduced. The mixture was refluxed (∼100 °C, 48 h) for acid hydrolysis. After cooling down to room temperature, the product was filtered through Buchner, rinsed with distilled water and dried in an oven (40 °C, overnight). Thereafter, the product was dissolved in NaOH (0.1 M), filtered and addition of HCl (4 M) to the filtrate led to a precipitate which was recovered after filtration (rinsed with distilled water to neutral pH). After repeating this step two more times and oven drying (40 °C, overnight), the yield was 57%.

Physicochemical characterization.— *Ultraviolet-visible (UV–vis) spectrometry.*—Experiments were performed in DMSO and in DMF using a 190 DES Double Energy System spectrophotometer.

Attenuated total reflection fourier-transform infrared spectroscopy (ATR-FTIRS).—The powder samples were deposited on a diamond crystal and the spectra, with a resolution of 4 cm^{-1}, were recorded on the Brucker TENSOR 27 FTIR spectrometer (materials synthesized in Burkina Faso) or on the Nicolet Nexus FTIR spectrometer (materials synthesized in France).

N_2 adsorption-desorption isotherms.—The surface properties [porosity and the specific surface area] were investigated by Brunauer–Emmett–Teller (BET) and distribution BJH measurements. N_2 adsorption-desorption isotherms were recorded at liquid N_2 temperature (77.3 K) using a Micrometrics ASAP 2020 instrument.

Scanning electron microscopy (SEM) and energy dispersive X-ray spectroscopy (EDX).—The morphology of the materials was analyzed by SEM on Hitachi S-4800 FEG. Semi-quantitative analysis was obtained by EDX analysis on the microscope ZEISS EVOHD 15, followed by 2D mapping of the different elements, C, N, O, Au and Cl. To enhance the imaging capability, a thin layer of Pt was coated on the samples.

C, H, N, S and O (CHNS-O) elemental analysis.—The CHNS-O analysis was performed on an Elementar vario MICRO cube.

High-resolution electrospray ionization mass spectrometry (HR-ESI-MS) analysis.—HR-ESI-MS analysis was performed with a Synapt G2-S mass spectrometer (Waters) equipped with an atmospheric pressure ionization source (API) pneumatically assisted with direct introduction (MS only) or flow injection analysis (FIA). Samples were ionized in positive electrospray (ESI) mode under the following conditions: electrospray voltage (ISV): 5500 V; orifice voltage (OR): 20 V; nebulizing gas pressure (air): 20 psi. The mass spectra were obtained with a time-of-flight analyzer (Q-TOF), resolution 30000. The exact mass measurement was performed in triplicate with a double internal calibration.

X-ray photoelectron spectroscopy (XPS).—XPS analysis was performed on a Thermo Electron ESCALAB 250 spectrometer equipped with a monochromatic radiation source Al Mono (Alkα = 1486.6 eV) operating at 150 W (15 kV and 10 mA). The measurements were performed directly on the samples in the form of powder arranged on a support in a chamber under high vacuum ($\leqslant 10^{-9}$ Torr): survey spectra at 1 eV per step for a transition energy of 150 eV and high-resolution spectra at 0.1 eV per step for a transition energy of 20 eV. The spectra are calibrated in binding energy with respect to the C 1 s energy of the C=C component at 284.4 eV. The charge is compensated by a low energy (−2 eV) electron beam. Quantification was performed from the peak area of the high-resolution spectra after correction with suitable sensitivity factors.

X-ray diffraction (XRD).—XRD patterns were recorded in a Bragg −Brentano mode (2θ = 2° to 60°) on a PANalytical X′Pert PRO diffractometer with Cu Kα radiation at the wavelength of 1.5406 Å, the voltage and tube current being 40 kV and 40 mA, respectively.

Electrochemical characterization in an aqueous medium.—*Catalytic ink preparation.*—Homogeneous catalytic ink was prepared by mixing the material (2 mg), DMF (180 μl) and a suspension of Nafion® (20 μl) in an ultrasonic water bath (20 min).[27] Next, an aliquot (6 μl) was pipetted onto the surface of the glassy carbon tip of a rotating disk electrode (RDE, 5 mm diameter) and dried under ambient conditions (leading to a material loading of 306 μg cm^{-2}). RDE was previously well-polished with alumina slurries (3 μm, 1 μm and 0.05 μm, successively) before washing with ultrapure water, and sonication in water (10 min). A polycrystalline gold electrode (RDE, 2 mm diameter) was used as the control electrode material.

Electrochemical measurements.—The electrochemical characterization was performed at 25 °C in a standard three-electrode and single compartment glass-cell using the potentiostat AUTOLAB PGSTAT128N (Metrohm, Netherlands). The reference electrode was Ag|AgCl|KCl (3 M), however, the potentials were calibrated to the reversible hydrogen electrode (RHE) according to the calibration relationship E(V vs RHE) = E(Ag/AgCl) + ΔE, ΔE = 0.235 V (please see details in Fig. S1 and accompanying comments). The counter electrode was a glassy carbon plate of large area (>5 cm^2). The electrolyte was 0.5 M H_2SO_4 (pH = 0.3), which was outgassed with Ar before measurements (20 min). The potentials range of CV was 0–1.6 V vs RHE, starting the scan at the open circuit potential (OCP) towards the upper potential limit (stable CV are reported, after 5 cycles). All CVs are iR-drop uncorrected. Current densities are normalized to geometric area.

Electrochemical characterization in a non-aqueous medium.—The solvent was DMSO, vacuum-dried over a molecular sieve 3 Å (100 °C overnight). The electrolyte was 0.1 M [^{n}Bu$_4$N][PF$_6$] and each compound [AuPc, AuPc(CN)$_8$, AuPc(COOH)$_8$] was fixed to 0.5 mM, except for blank experiments. The electrochemical characterization was performed at 25 °C in a standard three-electrode and single compartment glass-cell using the potentiostat AUTOLAB PGSTAT128N (Metrohm, Netherlands). The cell content was outgassed with Ar before measurements (20 min). The reference electrode was the commercial "RE-7 non aqueous reference electrode" from *BAS Inc.* (Ag/AgNO$_3$, 0.01 M AgNO$_3$ + 0.1 M [^{n}Bu$_4$N][PF$_6$] in acetonitrile). The counter electrode was a glassy carbon plate of large area (>5 cm^2). The working electrode was a glassy carbon (tip of a RDE, 3 mm diameter), which was polished (see above). For control experiments, a polycrystalline gold electrode (RDE, 2 mm diameter) was used as the working electrode. Starting the scan at OCP towards the upper potential limit, two electrode potential ranges of CV (stable CV are reported, after 2 cycles) were probed, (i) from −2.2 to 0 V vs Ag/AgNO$_3$, and (ii) from −2.2 to +0.5 V vs Ag/AgNO$_3$. All CVs are iR-drop uncorrected. Current densities are normalized to geometric area.

Results and Discussion

Spectrometry, spectroscopy and thermal stability studies.—We initially used UV–vis spectrometry to characterize the developed materials, as the ground state electronic spectra of the MPc have unique characteristic absorption.[1,2,15,24] For example, the intense Q-band is between at 662 nm (first synthesis of AuPc in 1995 by MacCragh and Koski, Scheme 1, without axial ligand X)[24] and 720 nm[1,2,15] is typical of the successful synthesis of a non-aggregated phthalocyanines. This main transition band Q conveys the charge transfer from the pyrrolic carbons to the other atoms of the macrocycle and is highly sensitive to changes on the macrocycle. Therefore, we performed UV–vis of the three materials AuPc, AuPc-(CN)$_8$ and AuPc-(COOH)$_8$ in two different organic solvents, in DMSO (Fig. 1a) and in DMF (Fig. 1b). The wavelengths of the main transition bands are reported in Table I. The profile of the spectra is characteristic of a gold phthalocyanine as reported for AuXPc (X = Cl, Br, etc.)[1,2] and the main positions are in agreement with the seminal results.[24] Basically, the two main absorption regions at 300–400 nm and at 600–800 nm correspond to the B-band and Q-band of metallophthalocyanines, respectively.[28–30] The 400–600 nm region is the valley of the ground-state linear absorption spectrum where the reverse saturation absorption occurs.[28]

For Q-band in DMSO, λ_{max} is nearly 680, 700 and 710 nm for AuPc, AuPc-(CN)$_8$ and AuPc-(COOH)$_8$, respectively. In comparison to AuPc, this represents a positive shift for the octa-substituted phthalocyanines by 20–30 nm. The shoulder appearing at 617 nm in the AuPc spectrum is located around 625 nm and 640 nm for AuPc(CN)$_8$ and AuPc(COOH)$_8$, respectively. Taken together, these results confirm the so-called "bathochromic effect" resulting from the successful substitution of peripheral hydrogens.[1,25,30]

Even though the introduction of carboxylic acid groups at the periphery significantly modifies the electronic properties of the macrocycle to accentuate the bathochromic shift, λ_{max} of AuPc is higher compared to others MPc (M = Fe, Co, etc.).[1,29,30] The results confirm that the bathochromic effect (or blue shift) increases with the atomic number of the central metal because of the change in the electronic configuration of the valence state. Also, the inter- and intramolecular interactions due to the presence of the carboxylic acid groups result in a dominant electron-donor effect leading to a shift of the overall bands towards higher wavelengths. The dipolar interactions and the formation of hydrogen bonds will stabilize the electron density around the macrocycle, and thus weakening the energy required for electronic transitions. Finally, a substitution at the periphery will allow to improve the solubility of the molecular material.[3,15,16]

We next used ATR-FTIRS to perform a deep characterization of the as-synthesized materials. Figure 1c shows the representative spectra, the full spectrum of the material AuPc(COOH)$_8$ is reported in Fig. S2. The vibrational frequencies of the characteristic bands of are gathered in Table S1. It is worth noting that the spectra of the octa-substituted AuPc(COOH)$_8$ and AuPc(CN)$_8$ materials are expected to be different from the spectrum of the unsubstituted AuPc. We note the disappearance, the appearance, the displacement as well as the variation of the intensity of certain bands. The changes in the domains of out-of-plane and in-plane C-H bond strain and elongation vibrations of the phthalocyanine macrocycle, 700–1000 cm^{-1} region, show that the nature of the bonds at the periphery of the macrocycle is different. Specifically, the band at 720 cm^{-1} for νC-H[23] decreases in intensity for AuPc(CN)$_8$ and AuPc(COOH)$_8$, which is explained by the substitution of half of the hydrogens of AuPc. The presence of a new band at 2220 cm^{-1}, assigned to the vibrational CN groups in MPc,[15,31,32] confirms the synthesis of the AuPc(CN)$_8$ material. The presence of this band in the spectrum of AuPc(COOH)$_8$ indicates the presence of the parent AuPc(CN)$_8$ and not a partial hydrolysis of all CN groups, since, as we will see later, the mass spectrometry confirms the expected mass. Compared to AuPc and AuPc(CN)$_8$, AuPc(COOH)$_8$ is characterized by new bands at 1703 and 1233 cm^{-1}, corresponding to νC=O and νC-O stretching vibrations.[31] From Fig. S2, the presence of the broad band between 2300 and 3600 cm^{-1} further corroborates the obtaining of the AuPc(COOH)$_8$ material. This band can be attributed to the elongation vibration (νO-H), in particular that of O-H groups involved in intra- and intermolecular hydrogen bonds.

We next used TGA-DTA to study the thermal behavior of the different materials prepared under two conditions: oxidative atmosphere (air) and inert atmosphere (N_2). The multifold objective was to know if the synthesis conditions were justified[7,16] and to anticipate the best conditions for the preparation of SACs or other calcined materials. Figure 1d displays the profiles of TGA-DTA from the room temperature to 800 °C (extended curves are reported in Figs. S3–S8). There is a notable difference between the unsubstituted gold phthalocyanine (AuPc), and the octo-substituted phthalocyanine [AuPc(CN)$_8$ (and AuPc(COOH)$_8$]. Below 300 °C, while there is no significant weight loss for AuPc, for AuPc(CN)$_8$ and AuPc(COOH)$_8$, a first weight loss occurs below 100 °C and a second one around 200 °C [AuPc(COOH)$_8$] and 250 °C

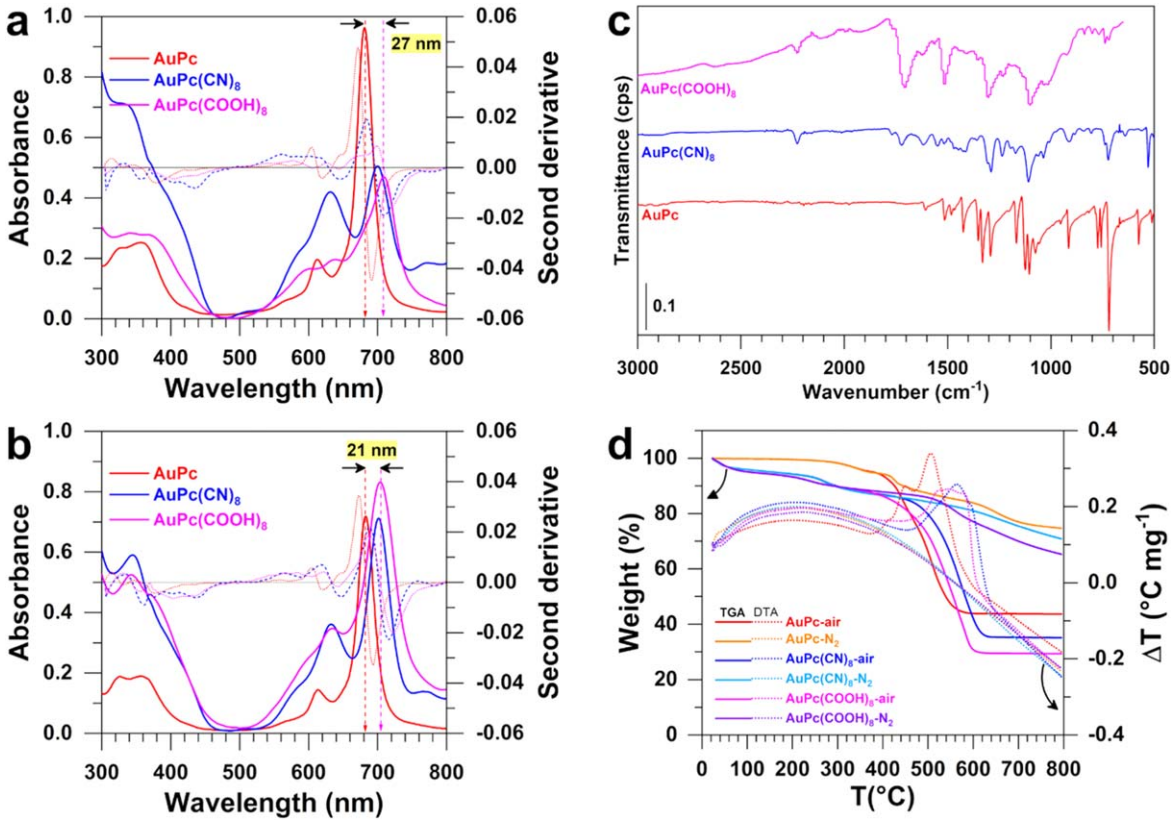

Figure 1. (a), (b) UV–vis in DMSO (a) and in DMF (b): spectra (solid lines, left-*y*) and second derivates (short dot lines, right-*y* axis). (c) ATR-FTIRS. (d) TGA (solid lines, left-*y*) and DTA (short dot lines, right-*y* axis) under air or nitrogen atmosphere (5 °C min^{-1}, 100 ml min^{-1}).

Table I. Physicochemical properties from UV–vis spectrometry.

Entry		AuPc	$AuPc(CN)_8$	$AuPc(COOH)_8$
DMSO	λ_{max}(nm)	319–352, 617, 680	338–368, 580, 625, 700	338–373, 588, 640, 707
DMF		325–345, 615, 680	346–371, 570, 622, 700	370, 585, 642, 702

[$AuPc(CN)_8$]. These endothermic behaviors could be attributed to the evaporation of water or solvent molecules that are adsorbed and/or trapped between the complexes as a result of an accentuated van der Waals interaction and require a much higher temperature to remove.[7,15,33] We note that the slight weight loss between 200 and 250 °C could be attributed to the initiation of the phthalocyanine degradation based on data obtained with other peripherally substituted MPc, such as the carboxyl dehydration.[15,34]

The temperatures higher than 300 °C correspond to the so-called extensive decomposition. The behavior is drastically different between N_2 and air; as expected, the thermal stability in air is lower than those under inert. For AuPc, the weight loss under air is 56 wt%, while it is 25 wt% under N_2. For $AuPc(CN)_8$, the mass loss is 65 wt% under air, while it is 29 wt% under N_2. For $AuPc(COOH)_8$ it is 71 wt% under air while it is 35 wt% under N_2. These trends are in agreement with the molecular weight of the three types of materials. Under both inert and oxidative conditions, octa-substituted phthalocyanines are more stable than the unsubstituted one: AuPc < $AuPc(CN)_8$ ≈ $AuPc(COOH)_8$. Previous works on other MPc (M = Cu, Fe, Co, and Ni) showed that the thermal stability increases with the atomic number of the central metal (due to the extent of covalent bonding of the metal ligand) as well as with substitution.[7,15] We note that the temperatures of the extensive decomposition region are higher than those found for other MPc containing substituted organic groups,[15,33] which could be explained by the higher atomic number of gold. Specifically, under oxidative conditions (air), DTA curves have two maxima, which could be assigned to the exothermic oxidative cleavage of the macrocycle, the oxidation of the cleavage products, and the oxidation of the central metal.[7]

Electron microscopy, textural, elemental and chemical analysis.—The above studies only show spectrometric and spectroscopic features that have qualitatively attested the preparation of AuPc-based materials. In order to obtain in-depth physicochemical data, we then carried out a series of complementary analyses. For morphology and composition, we performed the first SEM-EDX studies to date for AuPc-based materials. Figure 2 shows the micrographs at different magnifications (extended images are reported in Fig. S9). We observed morphological differences between the different materials, which could be explained by the self-assembly mode of the different molecules and the existence of inter- and intramolecular interactions. We note that the powders of each material were ground in a mortar before the microscopic observations. Although this operation can lead to a faceting bias, the formation of micro-scale platelets is obvious, especially for AuPc. For $AuPc(CN)_8$ and $AuPc(COOH)_8$, more aggregated spherical shapes forming large clusters appear.

We then collected 2D maps from the EDX analysis to determine the qualitative proportion and distribution of the different elements within the as-synthesized material. Figure 3 shows the resulting maps and histograms of atomic composition (Fig. S10 reports the extended SEM-EDX mapping). Visually, the mapping clearly

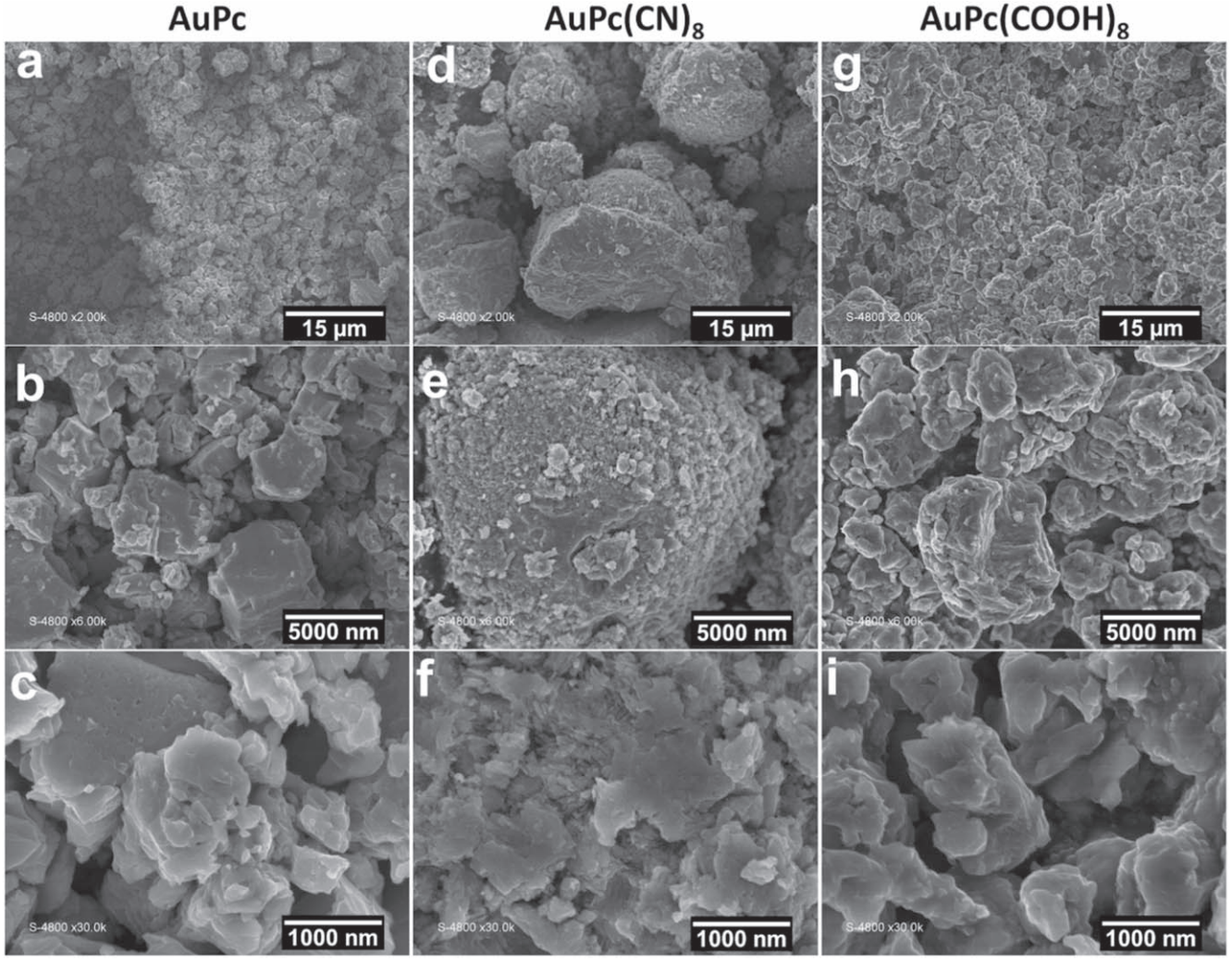

Figure 2. Representative SEM images of the synthesized materials at different magnifications: (a) AuPc, (b) $AuPc(CN)_8$ and (c) $AuPc(COOH)_8$.

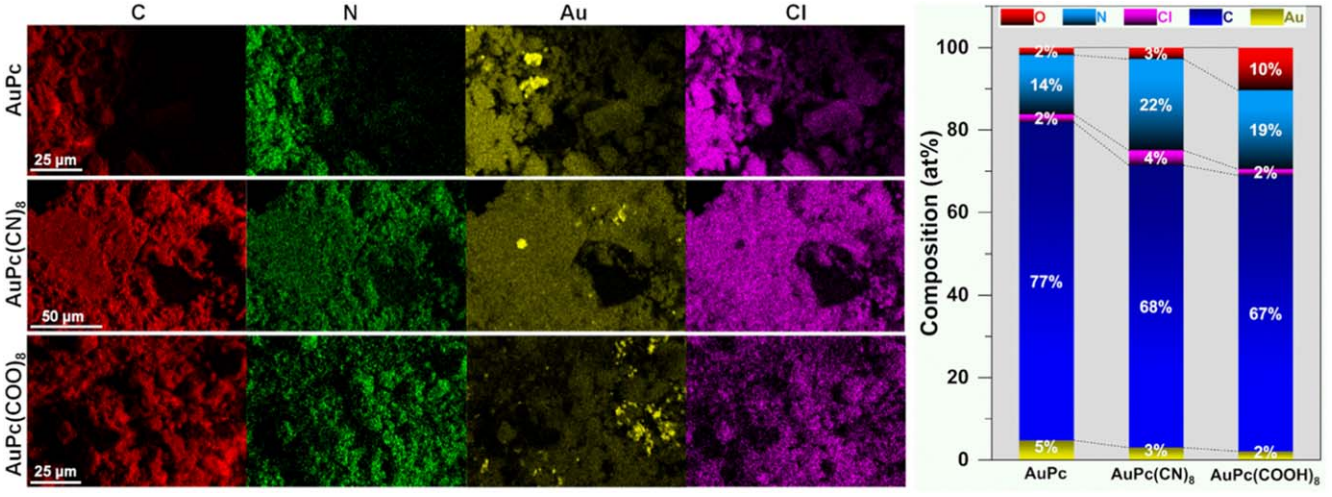

Figure 3. SEM-EDX mapping of different elements and the corresponding quantitative data.

highlights the formation of a material consisting of C, N, Au and Cl. (H is too light to be quantified by electron microscopy). A closer look at the Au images and the quantitative data allows us to rule out the hypothesis of the presence of the unreacted gold salt $HAuCl_4$ or the formation of AuCl, since the more intense areas should overlap with those of Cl and the Au/Cl ratio does not match. For gold maps, the presence of these areas of high intensity are therefore certainly made up of aggregates of metallic gold, implying that the synthesis conditions could be reducing. Otherwise, the dismutation of gold(I) organic and/or inorganic complexes could produce metallic gold, for

example $3AuCl_2^- \rightleftarrows AuCl_4^- + 2Au + 2Cl^-$, which is well-known in aqueous media ($K = 10^8$ at 25 °C).[35] We have not yet found a suitable solution to avoid this phenomenon, because if it were an MPc with a non-noble metal in the center, acid treatment would have been effective. Centrifuging would be one way to separate, however, the complete dissolution in an organic solvent remains an unsolved challenge for an unsubstituted MPc such as AuPc.[3,15–17]

The increase in N content in $AuPc(CN)_8$ compared to AuPc confirms the introduction of nitrogen. Similarly, the increase in O for $AuPc(COOH)_8$ compared to $AuPc(CN)_8$ endorses a hydrolysis of $AuPc(CN)_8$ to $AuPc(COOH)_8$. From Scheme 1, 1Au atom per 32 C, 1Au per 8 N and 1 N atom per 4 C were expected for the unsubstituted AuPc. The experimental fractions are slightly different but very close for octa-substituted $AuPc(CN)_8$ and $AuPc(COOH)_8$. Complementary CHNS-O analysis (Table S2) confirms the experimental trends, where the C/H atomic ratio for AuPc was 2.1 ± 0.1 (theoretically, C/H = 2). Overall, the differences could be explained by the presence of metallic gold clusters, reaction by-products as well as water molecules trapped in the molecular structures as shown by the TGA-DTA characterization.

Having shown that C, N, H and Au are within the chemical structure of the synthesized materials, we next used MS to determine the chemical structure. The HR-ESI-MS results are reported in Figs. S11–13 for the predicted structure and the experimental one. For AuPc, *m/z* $[M^+ - Cl]$ = 709.1171 (calculated: 709.1163) is in agreement with the previous reports.[1,2] For $AuPc(CN)_8$, *m/z* $[M^+ - Cl]$ = 909.0809 (calculated: 909.0783), and for $AuPc(COOH)_8$, *m/z* $[M^+ - Cl]$ = 1061.0309 (calculated: 1061.0350). Combining the different results, we can conclude that the prepared materials are composed of gold phthalocyanine (III) complexes containing a chloride ligand on the central atom, i.e. Au. This conclusion does not completely exclude a possible co-forming of the putative gold phthalocyanine (II), whose synthesis has never been replicated[1,20] after the first and the only report[24] back to 1965 by MacCragh and Koski. So far, only the alternative porphyrin pathway has provided access to a mononuclear gold(II) complex.[21]

Although existing work on gold phthalocyanines has not done so to date, we sought to obtain more textural properties by using N_2 as a probe molecule. Figure S14 and Table S3 report the obtained results. In Fig. S14a, the profile of the isotherms and the hysteresis loop at higher pressure due to capillary condensation reveals the presence of mesopores and microporous,[36] which is confirmed by the pore sizes distribution (Figs. S14b–S14c). A close examination of the N_2 adsorption-desorption isotherms (Fig. S14a) revealed an unusual behavior, namely the decrease of the adsorbed/desorbed volumes with increasing pressure. A plausible explanation is the amorphous character of the materials induced by these particular experimental conditions, which could lead to changes in the structural arrangement. Finally, the determined specific surface area (Brunauer–Emmett–Teller, BET)[37] is S_{BET} ($m^2\ g^{-1}$) = 2.35 ± 0.11 (AuPc), 2.42 ± 0.05 [$AuPc(CN)_8$], and 1.29 ± 0.07 [$AuPc(OOH)_8$]. To our knowledge, there are no values in the literature for gold phthalocyanine to use as a comparison. These values are low compared to traditional carbonaceous materials (tens or even hundreds of $m^2\ g^{-1}$),[38–40] which can be explained by the morphology of the materials and the high molar weight of gold.

Surface state analysis by XPS.—We then used XPS to carefully study the missing surface composition, the oxidation state of the elements, and the electronic interactions between the elements within the as-synthesized AuPc-based materials. Indeed, to the best of our knowledge, these critically important data are missing from the existing literature on gold phthalocyanines.[1,2,23–25] Herein, two types of XPS analysis were carried out. Firstly, we used the survey spectra to identify the different elements (bearing in mind that XPS analyses are limited to a few nm). Secondly, as to our knowledge there are no XPS data on gold phthalocyanines, based on the results of the previous characterizations, we proposed a set of detailed analyses of the high-resolution core level spectrum for each element to deduce the oxidation states and any electronic interactions.

Figure 4a shows the survey XPS spectra of the as-synthesized materials while the extracted quantitative data are reported in Fig. 4b. The constituent elements are C, N, Au and Cl, apart from hydrogen, which cannot be studied by XPS but whose presence has been previously confirmed by elemental analysis (CHNS-O directly and MS indirectly). This confirms the previous EDX results. Although it is well known that exposure to air causes surface oxidation (known as the passivation layer for metals), there is a clear increase in surface oxygen content in $AuPc(COOH)_8$. This may indicate successful conversion of $AuPc(CN)_8$ to $AuPc(COOH)_8$. Moreover, even though we observed the presence of some metallic gold aggregates by SEM-EDX, the evolution of the atomic proportions between chlorine and gold in Fig. 4b suggests the presence of the Cl ligand on Au in the phthalocyanine structure (cf Scheme S1). This would be in agreement with the previous results of high resolution mass spectrometry. Figure 5 shows the high-resolution XPS of C 1 s, N 1 s, Cl 2p and Au 4 f based on the binding energies (BEs) from the NIST SRD 20 v4.1 data-bank of XPS measured BEs (Table S4),[41] event thought has some uncertainties.[42] Starting from the low BEs to the high ones, Fig. 5a exhibits four peaks (for AuPc, the 1st peak of low intensity is not shown). Specifically, for AuPc,

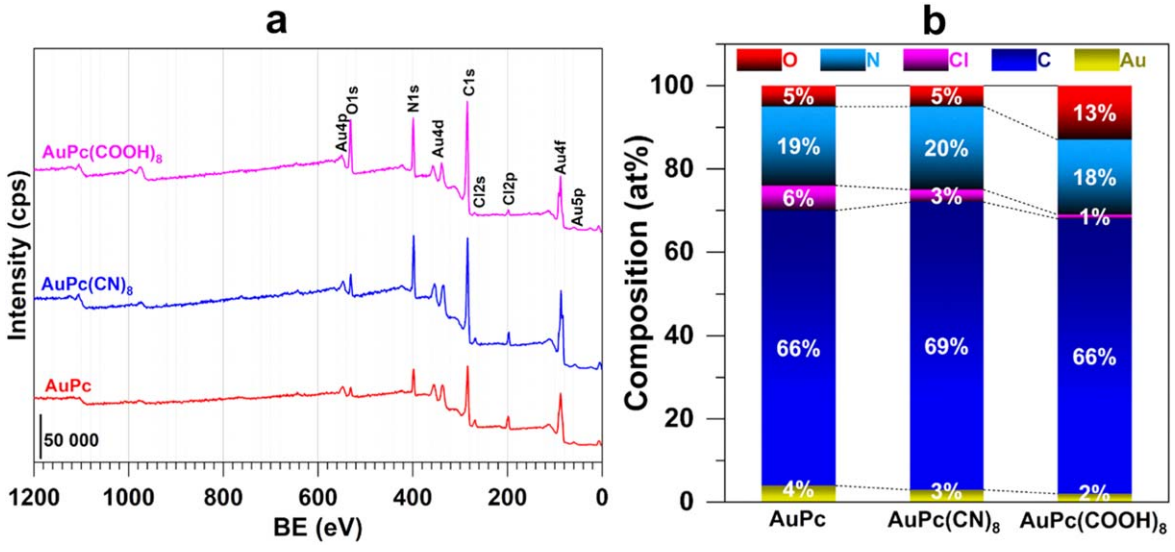

Figure 4. (a) Survey XPS spectra of the as-synthesized materials. (b) Overall surface atomic composition.

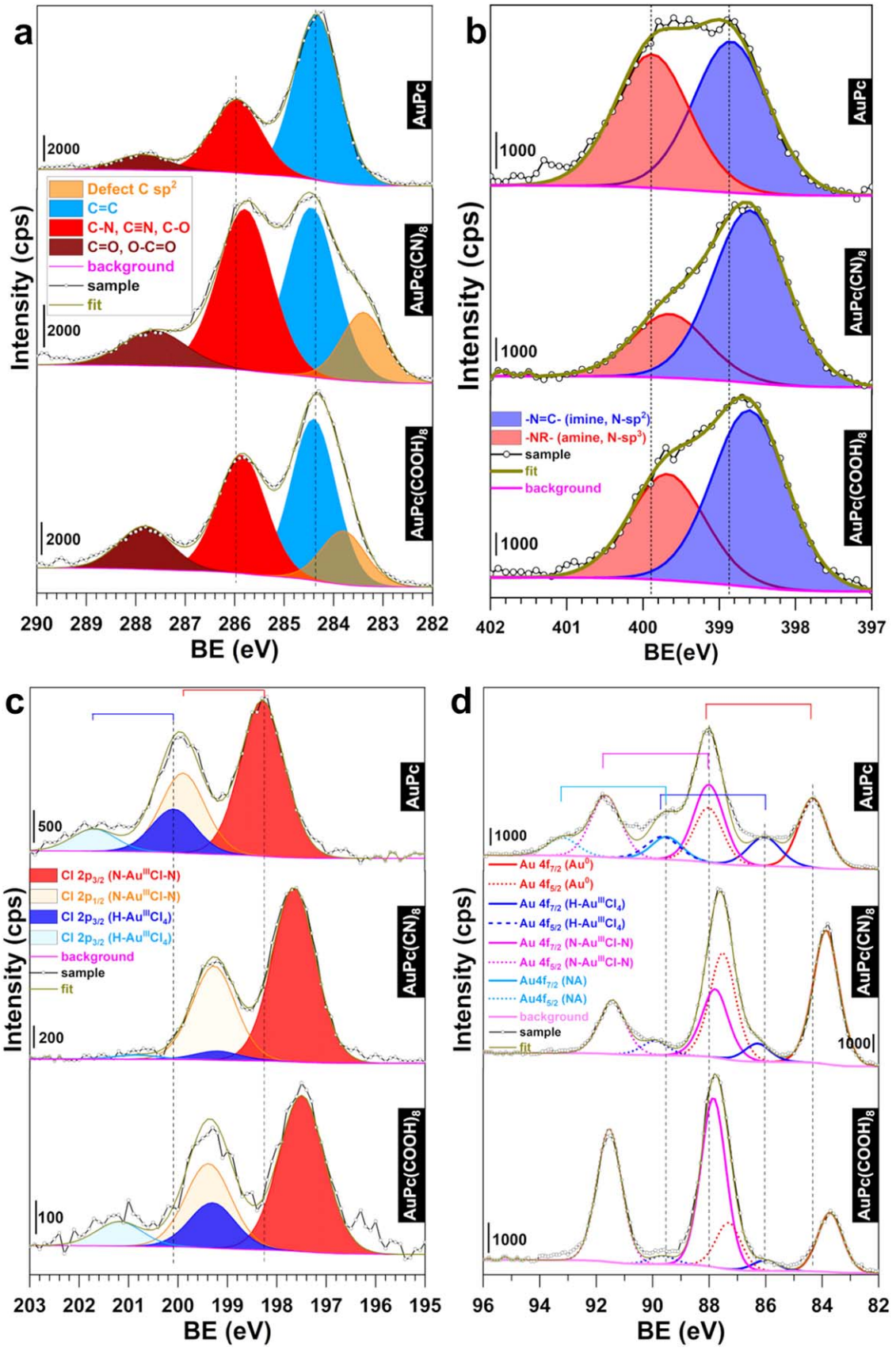

Figure 5. High-resolution XPS of (a) C 1 s, (b) N 1 s, (c) Cl 2p and (d) Au 4 f.

the peaks at 284.3 eV (FWHM = 1.19 eV; at% = 63), 285.9 eV (FWHM = 1.3 eV; at% = 30), and 287.9 eV (FWHM = 1.5; at% = 7) are unambiguously assigned to C=C, C–N/C≡N/C–O and, C=O/O–C=O, respectively.[41]

For $AuPc(CN)_8$ and $AuPc(COOH)_8$ materials, the obvious peak at 283.4–283.8 eV (FWHM = 1.1; at% = 14) has been previously reported for 2D graphene-based materials and has been assigned to defect C sp^2.[43,44] For $AuPc(CN)_8$, the surface composition is 38, 38, 10 and 14 at% for C=C, C–N/C≡N/C–C, C=O/O–C=O, and defect C sp^2, respectively [41, 13, 33 and 13 at% for $AuPc(COOH)_8$]. Even though a clear understanding of the differences between C–N and C≡N bonds is often deemed difficult,[45,46] our three materials constitute a set of control experiments to capture any influence of C≡N. Indeed, by comparing the three spectra, one can logically deduce that the steep signal change at 285.6–285.9 eV for $AuPc(CN)_8$ is due to a strong contribution of C≡N (C sp), which could not be solved by N 1 s. Indeed, the BE of C≡N (N sp) of 397–400 eV falls in the ranges of -N=C- (imine, pyridinic-N, N sp^2) at 398.3–398.5 eV and -NR- (N sp^3, amine, pyrrolic-N) at 399.8–399.9 eV.[41,47]

Specifically, the fitting of the N 1 s spectrum of AuPc (Fig. 5b) shows two peaks at 398.85 eV (FWHM = 1.2 eV; at% = 53), and 399.88 eV (FWHM = 1.1 eV; at% = 47), which correspond to the pyridinic-N and pyrrolic-N of the phthalocyanine macrocycle (cf Scheme S1), respectively. For $AuPc(CN)_8$, the surface composition is 73 and 27 at% for pyridinic-N and pyrrolic-N, respectively [62, 38 at% for $AuPc(COOH)_8$]. Furthermore, we observe a shift in the energy level for the octa-substituted $AuPc(X)_8$ (X = CN, COOH). This would imply that the peripheral substitution, even if it occurs far from the N-sp^3 and N-sp^2 close to the inner part of the macrocycle, generates an electronic delocalization. The latter is even more true considering the UV–vis features that suggested such a hypothesis.

The high-resolution XPS of the Cl 2p is displayed in Fig. 5c where each pair of peaks is due to Cl $2p_{3/2}$ and Cl $2p_{1/2}$ spin–orbit coupling. Basically, the metal chloride (e.g. Cl-Au) is expected at 198–200 eV and the organic chloride (e.g. C-Cl) is expected at 200–202 eV for Cl $2p_{3/2}$.[41] Based on existing data on chlorinated gold species, a common interpretation is made with Au 4 f.[48–56] It has been reported that Cl $2p_{3/2}$ appears around 200.1 eV in a tetrachloroaurate environment ($HAuCl_4$) while for a low chlorine content such as Au(I)-Cl complexes lead to Cl $2p_{3/2}$ at a lower BE of 199.5 eV.[48] Consequently, for AuPc, the peak at 198.3 eV (FWHM = 1.1 eV; at% = 78) and 200.1 eV (FWHM = 1.1; at% = 22) could be assigned, respectively, to Cl bonded to Au in the phthalocyanine referred to as N-Au^{III}Cl-N (Scheme 1, with an axial ligand Cl) and the few residual traces of the $HAuCl_4$ precursor (given that XPS is a highly sensitive surface technique). These two assignments are in agreement with the results Au 4 f spectra (Fig. 5d). Indeed, for AuPc, the peak at 86.1 eV (FWHM = 1.3 eV) corresponds to Au $4f_{7/2}$ of $XAu^{III}Cl_4$ (X = H, Na, K).[48–50] The peak at 84.3 eV (FWHM = 1.2 eV) belongs to Au $4f_{7/2}$ of metallic gold, which can come from the observed aggregates in SEM-EDX images as well as photo-reduction of gold (I/II/III) species by the photo-emission process during XPS analysis.[53–58] The peak at 88.0 eV (FWHM = 1.2 eV) for AuPc can be assigned to Au $4f_{7/2}$ of gold (III) surrounded by nitrogen and chlorine in N-Au^{III}Cl-N (Scheme 1, with an axial ligand Cl). We note that due to the overlap with the dominant pyridinic-N and pyrrolic-N moieties of the phthalocyanine macrocycle, the previous N 1 s could not provide access to an N-Au bond. As explained above, the shifts in the energy levels of Cl 2p and Au 4 f for the octa-substituted $AuPc(X)_8$ (X = CN, COOH) could be the result of the peripheral substitution, which generates an electronic delocalization and makes the metallophthalocyanines unique materials for many photo, optical, electrical, catalytic applications.[1–3,5,6,8] Finally, the peak of Au $4f_{7/2}$ at 89.5 eV (FWHM = 1.2 eV) of low contribution in the octa-substituted $AuPc(X)_8$ (X = CN, COOH) materials is actually unknown. It could be hypothesized that this is the signature of the putative gold (II) phthalocyanine,[1,20,24] where the absence of the chlorine ligand on the central atom would lead to a strengthening of the Au-N bond and thus higher binding energies. As previously explained, the only report[24] claiming the isolation of gold (II) phthalocyanine did not perform any XPS analysis and attempts to reproduce or replicate the synthesis failed.[1]

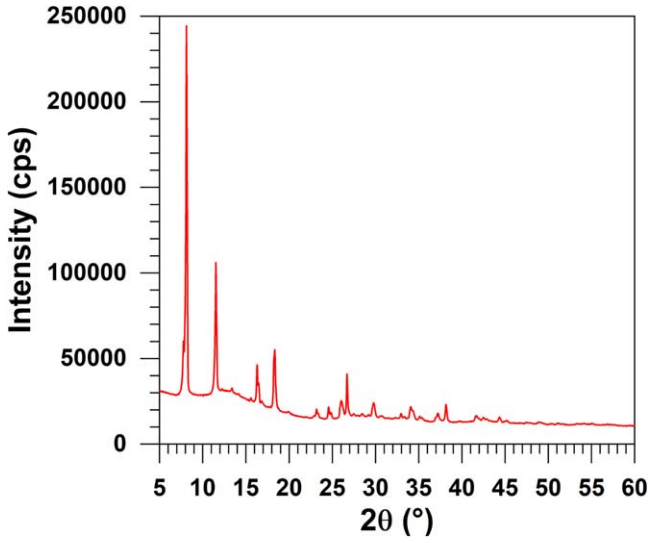

Figure 6. XRD patterns of the synthesized gold phthalocyanine material, AuPc.

X-ray diffraction.—In the case of AuPc, we had sufficient material to obtain useable diffraction patterns, which to our knowledge is the first study performed for gold phthalocyanine. Figure 6 shows five main diffraction peaks at 7.1°, 11.5°, 16.2°, 18.3° and 26.5°, which clearly confirm that the synthesized AuPc material has a crystalline and ordered structure. Compared to other MPc materials, these peaks could be assigned to the α polymorphic form of the phthalocyanine.[2,59–62] We note that the crystallographic orientation is material dependent and difficult to assign since the positions are very close. For example, Li et al.[63] have synthesized metal-free phthalocyanine α-H_2Pc and observed diffraction peaks at 6.8°, 14.9°, and 26.4°, which were assigned to (200), (004), and (113) crystal planes of α-H_2Pc (standard JCPDS card No. 36–1882, space group: C2/n). Basova et al.[2] reported an AuPc (with an axial Cl ligand) with a main diffraction peak at 7°, which they attributed to the (100) lattice plane and the edge-on orientation of the MPc molecules.

In conclusion, all these physicochemical characterizations have demonstrated the successful preparation of gold phthalocyanine, which could potentially be used directly in (photo)electrochemical applications. Another possibility is to obtain, after thermal treatment, nanostructured gold on a nitrogen-doped carbon framework or a single atom catalyst (SAC) where a single Au atom will be embedded in a nanostructured carbon-nitrogen scaffold.

Electrochemical investigation.—So far, the previous sections have provided new insights into gold phthalocyanine by means of SEM-EDX, BET, XPS and XRD, in addition to the usual UV–vis, FTIRS and MS analysis. Finally, to interrogate the redox properties, we used cyclic voltammetry (CV). For this purpose, we performed multivariate study using 0.5 M H_2SO_4 (in water) and 0.1 M [^{n}Bu_4N][PF_6] (in DMSO) as model electrolytes for the aqueous and non-aqueous media, respectively. We can confirm that the synthesized AuPc and its derivates are not soluble in the used 0.5 M H_2SO_4 electrolyte.

Figures 7a–7c show the voltammograms at different scan rates according to IUPAC convention ($j > 0$ for oxidation and $j < 0$).[64] Control experiments are reported in Figs. S15–S16. While the same amount of material was deposited on the electrode in each case, there

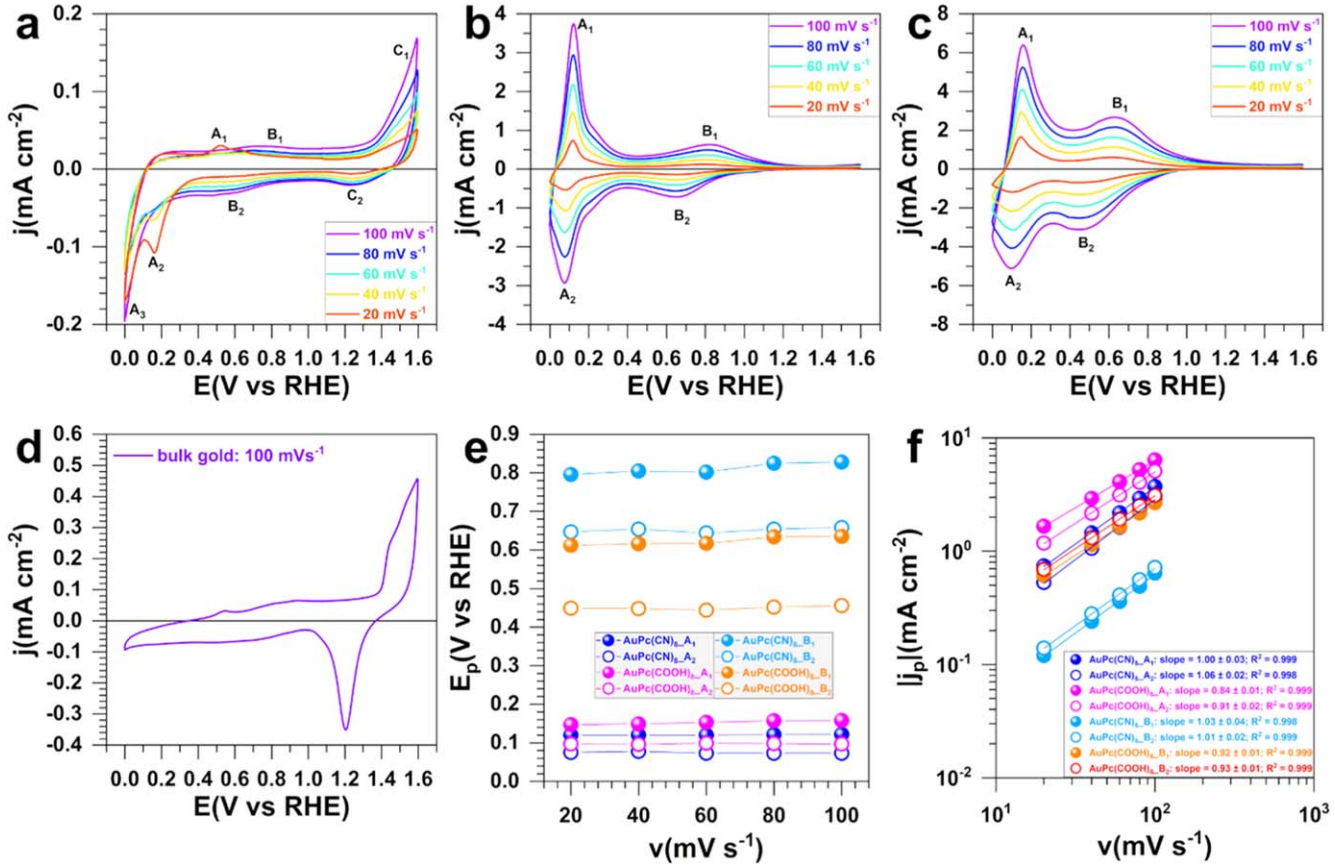

Figure 7. Electrochemistry in an aqueous medium (Ar-saturated 0.5 M H_2SO_4 at 25 °C). (a)–(c) CVs at different scan rates: (a) AuPc, (b) $AuPc(CN)_8$ and (c) $AuPc(COOH)_8$. (d) CV of bulk gold at 100 mV s^{-1}. (e) Plots of the potential of the peaks as a function of the scan rate. (f) Plots of the peak current density vs the scan rate on a log−log scale. Note: "blank" refers to glassy carbon without the ink deposit (material loading of 306 μg cm^{-2}).

is a clear difference between the unsubstituted (Fig. 7a) and the octo-substituted gold phthalocyanines (Figs. 7b–7c). The character linked to the low solubility of the non-substituted MPc[3,15–17] could be the reason for the low current density AuPc material, although in this case catalytic inks have been prepared instead of a homogeneous phase electrochemistry. The extracted electrochemical properties are gathered in Table S5. Ideally, a metal-free phthalocyanine α-H_2Pc would serve as a reference material for the assignment of the redox waves. However, the complexity of the synthesis led us to stick to the three materials AuPc, $AuPc(CN)_8$ and $AuPc(COOH)_8$, which are known from previous characterizations to have an axial Cl ligand on the central atom. We used bulk gold as a control material (Fig. 7d), which can help to rule out the hypothesis that the redox peaks originate from a few gold particles, as suggested by previous characterizations. By comparing Figs. 7a–7c and Fig. 7d, we propose that the redox process marked by C_1/C_2 (potentials higher than 1.1 V vs RHE), which is similar to the behavior of gold in acidic media, could be attributed to the observed metallic gold (based on SEM-EDX and XPS). Another possibility is the irreversible bulk reduction of the AuPc to metallic gold, which has been observed on PtPc.[65] The nearly reversible redox pair A_1/A_2 between 0.08 and 0.15 V vs RHE in $AuPcX_8$ (X = CN, COOH) materials is in the same potential window as the previous observations with CuPc.[32,61] Based on the potential of the peaks as a function of the scan rate (Fig. 7e and Table S5), the peak-to-peak potential difference of ΔE_p = 40–-60 mV suggests that the involved number of electrons is between 1 and 2.[66] Besides, the redox pair B_1/B_2 between 0.60 and 0.81 V vs RHE has ΔE_p = 163–170 mV, which is characteristic of the transfer of 1 electron with a much lower electrochemical kinetics. Indeed, the analysis of the peak current density vs the scan rate (Figs. 7f and S16) demonstrates that the electrochemical process is in a mixed regime of adsorption and diffusion.[66–68] Leveraging on the existing electrochemistry literature of other metallophthalocyanines[32,61,69–71] and gold porphyrin,[21,22] we postulated that the observed redox peaks are due to the three states of the phthalocyanine ring reduction and oxidation AuPc/$[AuPc]^-$, $[AuPc]^-/[AuPc]^{2-}$ and $[AuPc]^{2-}/[AuPc]^{3-}$.

The CVs at 100 mV s^{-1} in DMSO + 0.1 M $[nBu_4N][PF_6]$ profiles of the different compounds (0.5 mM) are reported in Figs. 8a–8c where the "blank" refers to the absence of compound. In order to rationally assign the different redox processes, we performed control experiments using a bare gold electrode, which is reported in Fig. 8d. While the redox pair C_1/C_2-C_2' is attributed to the behavior of gold (oxidation in C_1 and reduction in C_2-C_2'), the unexpected redox pair A_1'/A_2' could be the trace amount of dissolved oxygen.[71] Similar to the above discussion in aqueous media,[32,61,69–71] we hypothesize that the other observed redox A_1/A_2 and B_1/B_2-B_2' peaks are due to the phthalocyanine ring reduction and oxidation, AuPc/$[AuPc]^-$, $[AuPc]^-/[AuPc]^{2-}$ and $[AuPc]^{2-}/[AuPc]^{3-}$. The discrepancy in the behavior of redox processes between aqueous and non-aqueous electrolytes could be explained by competitive HER in aqueous media that reduce the potential window where we could observe all redox processes. A possible solution to widen the electrochemical window by mitigating HER (and OER) could be an imidazolium chloride-based aqueous electrolyte as demonstrated by Huang et al.[72] for Ni and Cu phthalocyanines. The second possible explanation is the difference between the rates of heterogeneous and homogeneous electrochemistry because the thermodynamics and kinetics of electron transfer processes are not the same for aqueous electrolytes where the materials have been deposited on the electrode, whereas in non-aqueous electrolytes, the materials are in the electrolyte. In

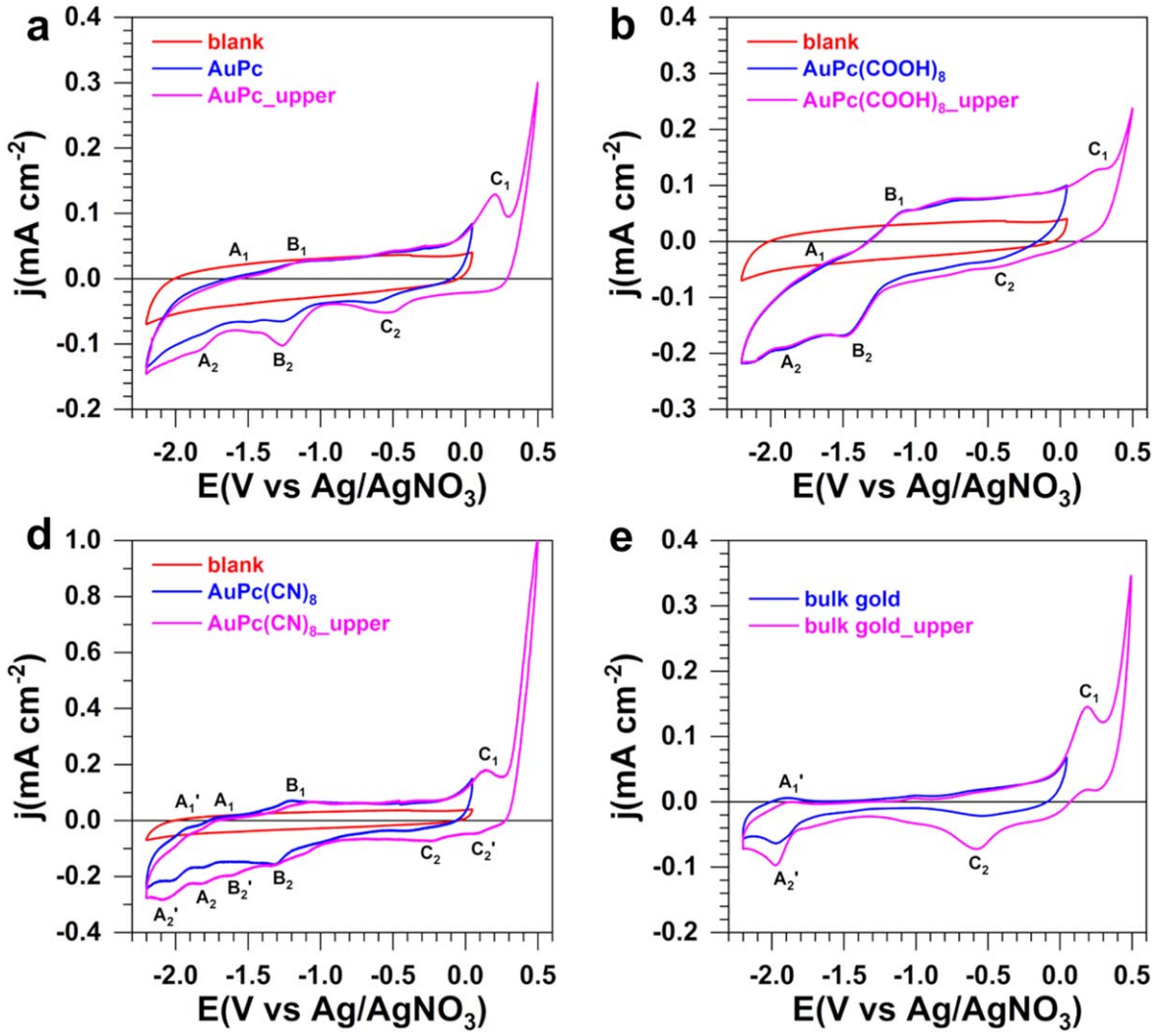

Figure 8. Electrochemistry in non-aqueous media (Ar-saturated 0.1 M [^{n}Bu$_4$N][PF$_6$] in DMSO, $C_{compound}$ = 0.5 mM, 25 °C). (a)–(c) Effect of upper potential limit for CVs (100 mV s^{-1}) of: (a) AuPc, (b) AuPc(CN)$_8$, (c) AuPc(COOH)$_8$, and (d) CV of bulk gold. The working electrode was a glassy carbon for (a)–(c) and "blank" refers to the absence of compound, i.e. $C_{compound}$ = 0 mM.

summary, these first results, both heterogeneous (catalytic ink for aqueous manipulations) and homogeneous (dissolution in organic solvents), reinforce our fundamental knowledge of the electrochemistry of gold phthalocyanines. They can therefore serve as a basis for the design of electrode materials for specific electrochemical reactions such as the two-electron ORR, as demonstrated by DFT calculations,[18] but also for consideration in photo-electrochemistry/photo-electrocatalysis.

Structures of the synthesized gold-based phthalocyanines.— Based on the various complementary and detailed physicochemical characterizations, Scheme 2 shows the structures of the synthesized phthalocyanines, AuPc (unsubstituted), AuPc(CN)$_8$ (octo-substituted CN groups) and AuPc(COOH)$_8$ (octo-substituted COOH groups). The proposed detailed synthetic routes are shown in Scheme S1. Although the synthesis of (unsubstituted) AuPc has been reported,[24] we developed a new synthetic methodology as with the octo-substituted ones. It is worth mentioning that this is the first time that the oxidation state of the different elements, morphology, composition and electrochemical properties are reported for gold phthalocyanine using XPS, SEM, EDX and cyclic voltammetry (aqueous and non-aqueous media. For example, XPS has provided molecular-level information on the structures of gold phthalocyanines involving Au-N and Au-Cl bonds, then suggesting that the "putative gold phthalocyanine,"[1,20,24] i.e. in the absence of the axial X ligand, is likely a mixture of gold(II) and gold(III) phthalocyanine complexes.

Conclusions

In summary, we have provided new physicochemical and electrochemical insights from the extensive investigation of three types of home-made gold phthalocyanines, namely the unsubstituted AuPc, and two octo-substituted AuPc(X)$_8$ (X = CN, COOH). We have integrated complementary methods (UV–vis, FTIRS, TGA-TDA, HR-ESI-MS, SEM-EDX, XRD, XPS, CV) to deeply examine the structures and the physical features. To date, we have obtained new results by using for the first time SEM-EDX, BET, XRD, XPS and CV (in both aqueous and non-aqueous media) techniques to study gold phthalocyanines.

Our results indicate that the central gold has an axial Cl. Although XPS at the Au 4 f core level may suggest its presence, our results did not allow conclusive evidence of the "putative gold (II) phthalocyanine,"[24] for which most previous attempts to isolate it have failed.[1,20] Furthermore, our new SEM-EDX 2D maps and XPS surface analysis protocols have provided molecular level insights into the Au-N and Au-Cl bonded gold phthalocyanine structures. Both XRD and CV have provided the first preliminary insights into the crystalline structure and the redox properties of gold

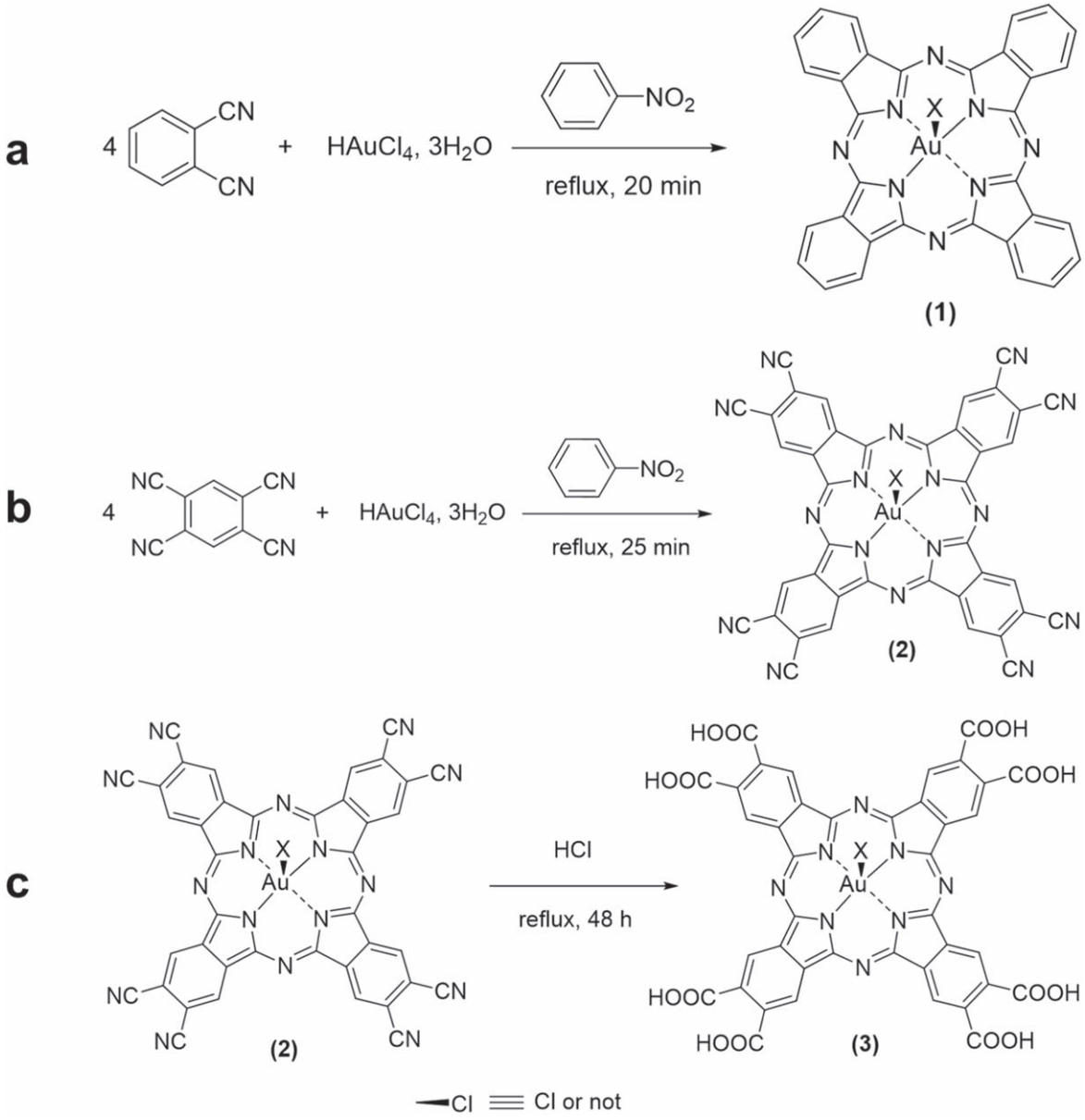

Scheme 2. Synthesis of gold-based phthalocyanines: (a) AuPc (unsubstituted, (1)), (b) $AuPc(CN)_8$ (octo-substituted CN groups, (2)) and (c) $AuPc(COOH)_8$ (octo-substituted COOH groups, (3)). Putative gold phthalocyanine is the absence of the axial ligand X.

phthalocyanines. By refining the local environment of gold within the phthalocyanine macrocycle, we have established an important benchmark for catalyzing the design of a new class of gold-based nanostructured materials for many applications such as (photo) electrocatalysis. The present fundamental knowledge of gold phthalocyanine can serve as a template for the development of the emerging new class of single atom catalysts (SACs), as our TGA-DTA-DSC results have improved our understanding of the thermal behavior of the materials. Indeed, it has been shown theoretically (density functional theory, DFT)[18] that, among 210 SACs models, Au-N_4-C SACs derived from gold phthalocyanines are not only thermodynamically and electrochemically stable, but, if experimentally synthesized, they could be suitable candidates for the sustainable and on-site electrocatalytic conversion of O_2 to H_2O_2.

Acknowledgments

W.-K. G. A. Nitiema gratefully acknowledges the financial support from Campus France for his stay at IEM Montpellier through the SCAC program. Y. H. acknowledge startup funds support from LabEx CheMISyst (ANR-10-LABX-05–01). We thank Didier Cot, Bertrand Rebiere, and Arie van der Lee from IEM Montpellier for assistance during SEM, EDX and XRD measurements. Magalie Lefeuvre (*Laboratoire de Mesures Physiques*, LMP, University of Montpellier, France) is acknowledged for CHNS-O analysis.

ORCID

Yaovi Holade https://orcid.org/0000-0002-8806-568X

References

1. E. W. Y. Wong, A. Miura, M. D. Wright, Q. He, C. J. Walsby, S. Shimizu, N. Kobayashi, and D. B. Leznoff, *Chem. Eur. J.*, **18**, 12404 (2012).
2. T. V. Basova, R. G. Parkhomenko, P. O. Krasnov, I. K. Igumenov, B. Kadem, and A. K. Hassan, *Dyes Pigm.*, **122**, 280 (2015).
3. T. Nyokong, *Coord. Chem. Rev.*, **251**, 1707 (2007).
4. S. Hebić, M. Bayo-Bangoura, K. Bayo, K. Servat, C. Morais, T. W. Napporn, and K. Boniface Kokoh, *J. Solid State Electrochem.*, **20**, 931 (2016).
5. S. Wei, H. Zou, W. Rong, F. Zhang, Y. Ji, and L. Duan, *Appl. Catal. B: Env.*, **284**, 119739 (2021).
6. M. Calvete, G. Y. Yang, and M. Hanack, *Synth. Met.*, **141**, 231 (2004).

7. D. Wöhrle and B. Schulte, *Makromol. Chem.*, **186**, 2229 (1985).
8. R. G. Parkhomenko, A. S. Sukhikh, D. D. Klyamer, P. O. Krasnov, S. Gromilov, B. Kadem, A. K. Hassan, and T. V. Basova, *J. Phys. Chem. C*, **121**, 1200 (2017).
9. C. A. Melendres and X. Feng, *J. Electrochem. Soc.*, **130**, 811 (1983).
10. C. A. Caro, J. H. Zagal, and F. Bedioui, *J. Electrochem. Soc.*, **150**, E95 (2003).
11. S. I. Mho, B. Ortiz, N. Doddapaneni, and S. M. Park, *J. Electrochem. Soc.*, **142**, 1047 (1995).
12. S. I. Mho, B. Ortiz, S. M. Park, D. Ingersoll, and N. Doddapaneni, *J. Electrochem. Soc.*, **142**, 1436 (1995).
13. A. Kotiaho, R. Lahtinen, A. Efimov, H.-K. Metsberg, E. Sariola, H. Lehtivuori, N. V. Tkachenko, and H. Lemmetyinen, *J. Phys. Chem. C*, **114**, 162 (2010).
14. D. Perilli, R. Breglia, and C. D. Valentin, *J. Phys. Chem. C*, **126**, 9615 (2022).
15. F. Hacıvelioğlu, M. Durmuş, S. Yeşilot, A. G. Gürek, A. Kılıç, and V. Ahsen, *Dyes Pigm.*, **79**, 14 (2008).
16. M. Sommerauer, C. Rager, and M. Hanack, *J. Am. Chem. Soc.*, **118**, 10085 (1996).
17. T. Basova, A. Hassan, M. Durmuſ, A. G. Gürek, and V. Ahsen, *Coord. Chem. Rev.*, **310**, 131 (2016).
18. X. Guo, S. Lin, J. Gu, S. Zhang, Z. Chen, and S. Huang, *ACS Catal.*, **9**, 11042 (2019).
19. J. Luo, M. Chen, Z. Zhang, K. Wang, S. Zhang, and S. Chen, *J. Phys. Chem. C*, **125**, 24988 (2021).
20. K. Heinze, *Angew. Chem. Int. Ed.*, **56**, 16126 (2017).
21. S. Preiß, C. Förster, S. Otto, M. Bauer, P. Müller, D. Hinderberger, H. Hashemi Haeri, L. Carella, and K. Heinze, *Nat. Chem.*, **9**, 1249 (2017).
22. S. Preiß, J. Melomedov, A. W. von Leupoldt, and K. Heinze, *Chem. Sci.*, **7**, 596 (2016).
23. A. Laguna and M. Laguna, *Coord. Chem. Rev.*, **193-195**, 837 (1999).
24. A. MacCragh and W. S. Koski, *J. Am. Chem. Soc.*, **87**, 2496 (1965).
25. B. Ouemega, M. Bayo-Bangoura, and K. Bayo, *J. Soc. Ouest-Afr. Chim.*, **031**, 42 (2011).
26. Z. Wang, L. Gu, L. Song, H. Wang, and R. Yu, *Mater. Chem. Front.*, **2**, 1024 (2018).
27. B. G. Pollet, *Electrocatalysis*, **5**, 330 (2014).
28. C. Li, L. Zhang, M. Yang, H. Wang, and Y. Wang, *Phys. Rev. A*, **49**, 1149 (1994).
29. W. Lu, B. Zhao, N. Li, Y. Yao, and W. Chen, *React. Funct. Polym.*, **70**, 135 (2010).
30. H. Xia and M. Nogami, *Opt. Mater.*, **15**, 93 (2000).
31. C.-X. Lü, G.-P. Zhan, K. Chen, Z.-K. Liu, and C.-D. Wu, *Appl. Catal. B: Env.*, **279**, 119350 (2020).
32. D. Wöhrle, V. Schmidt, B. Schumann, A. Yamada, and K. Shigehara, *Ber. Bunsen-Ges. Phys. Chem.*, **91**, 975 (1987).
33. R. Seoudi, G. S. El-Bahy, and Z. A. El Sayed, *J. Mol. Struct.*, **753**, 119 (2005).
34. V. Ahsen, E. Yilmazer, M. Ertas, and Ö. Bekâroğlu, *J. Chem. Soc., Dalton Trans.*, **2**, 401 (1988).
35. J. J. Lingane, *J. Electroanal. Chem.*, **4**, 332 (1962).
36. K. Sing, D. Everett, R. Haul, L. Moscou, R. Pierotti, J. Rouquerol, and T. Siemieniewska, *Pure Appl. Chem.*, **57**, 603 (1985).
37. S. Brunauer, P. H. Emmett, and E. Teller, *J. Am. Chem. Soc.*, **60**, 309 (1938).
38. H. J. Mackintosh, P. M. Budd, and N. B. McKeown, *J. Mater. Chem.*, **18**, 573 (2008).
39. M. Ladouceur, G. Lalande, D. Guay, J. P. Dodelet, L. Dignard-Bailey, M. L. Trudeau, and R. Schulz, *J. Electrochem. Soc.*, **140**, 1974 (1993).
40. C. Domínguez, F. J. Pérez-Alonso, M. Abdel Salam, J. L. Gómez de la Fuente, S. A. Al-Thabaiti, S. N. Basahel, M. A. Peña, J. L. G. Fierro, and S. Rojas, *Int. J. Hydrogen Energy*, **39**, 5309 (2014).
41. A. V. Naumkin, A. Kraut-Vass, S. W. Gaarenstroom, and C. J. Powell, (2012)"NIST X-ray photoelectron spectroscopy database, NIST standard reference database 20, version 4.1." *US Department of Commerce, Washington*, Accessed 2023.02.15.
42. B. V. Crist, *J. Electron. Spectrosc. Relat. Phenom.*, **231**, 75 (2019).
43. P. R. Kidambi, B. C. Bayer, R. Blume, Z.-J. Wang, C. Baehtz, R. S. Weatherup, M.-G. Willinger, R. Schloegl, and S. Hofmann, *Nano Lett.*, **13**, 4769 (2013).
44. I. Abidat et al., *Carbon*, **111**, 849 (2017).
45. D. Zeng, K. C. Yung, and C. Xie, *Surf. Coat. Technol.*, **153**, 210 (2002).
46. P. Hammer, R. Lacerda, R. Droppa Jr, and F. Alvarez, *Diam. Relat. Mater.*, **9**, 577 (2000).
47. A. Majumdar, S. C. Das, T. Shripathi, and R. Hippler, *Compos. Interfaces*, **19**, 161 (2012).
48. Y. Mikhlin, A. Karacharov, M. Likhatski, T. Podlipskaya, Y. Zubavichus, A. Veligzhanin, and V. Zaikovski, *J. Colloid Int. Sci.*, **362**, 330 (2011).
49. Y. Gao and L. Torrente-Murciano, *Nanoscale*, **12**, 2740 (2020).
50. P. Londoño-Larrea, J. P. Vanegas, D. Cuaran-Acosta, E. Zaballos-García, and J. Pérez-Prieto, *Chem. - Eur. J.*, **23**, 8137 (2017).
51. Y. Geng, M. Liu, J. Xue, P. Xu, Y. Wang, L. Shu, Q. Zeng, and C. Wang, *Chem. Commun.*, **51**, 6820 (2015).
52. J. Mycroft, G. Bancroft, N. McIntyre, and J. Lorimer, *Geochim. Cosmochim. Acta*, **59**, 3351 (1995).
53. J.-P. Sylvestre, S. Poulin, A. V. Kabashin, E. Sacher, M. Meunier, and J. H. Luong, *J. Phys. Chem. B*, **108**, 16864 (2004).
54. X. Zhao, Q. Wang, X. Zhang, Y.-I. Lee, and H.-G. Liu, *Phys. Chem. Chem. Phys.*, **18**, 1945 (2016).
55. D. W. Hatchett, M. Josowicz, J. Janata, and D. R. Baer, *Chem. Mater.*, **11**, 2989 (1999).
56. Gold—XPS Analysis - Cardiff University, in, http://sites.cardiff.ac.uk/xpsaccess/reference/gold/ (Accessed 23 February 2023).
57. Y.-Y. Fong, B. R. Visser, J. R. Gascooke, B. C. Cowie, L. Thomsen, G. F. Metha, M. A. Buntine, and H. H. Harris, *Langmuir*, **27**, 8099 (2011).
58. Q. Li, K. Bi, Y. Niu, S. Zhou, L. Tan, J. Mu, S. Han, S. Zhang, W. Geng, and L. Mei, *Opt. Express*, **30**, 40482 (2022).
59. P. Ballirano, R. Caminiti, C. Ercolani, A. Maras, and M. A. Orru, *J. Am. Chem. Soc.*, **120**, 12798 (1998).
60. B. B. Topuz, G. Gündüz, B. Mavis, and Ü. Çolak, *Dyes Pigm.*, **96**, 31 (2013).
61. K. Patil, S. Sathaye, R. Hawaldar, B. Sathe, A. Mandale, and A. Mitra, *J. Colloid Int. Sci.*, **315**, 747 (2007).
62. A. Sukhikh, D. Bonegardt, D. Klyamer, P. Krasnov, and T. Basova, *Molecules*, **25**, 1620 (2020).
63. X. Li, Y. Feng, C. Li, H. Han, X. Hu, Y. Ma, and Y. Yang, *Green Process. Synth.*, **10**, 95 (2021).
64. N. Elgrishi, K. J. Rountree, B. D. McCarthy, E. S. Rountree, T. T. Eisenhart, and J. L. Dempsey, *J. Chem. Educ.*, **95**, 197 (2017).
65. R. J. C. Brown, A. R. Kucernak, N. J. Long, and C. Mongay-Batalla, *New J. Chem.*, **28**, 676 (2004).
66. A. J. Bard and L. R. Faulkner, *Electrochemical Methods: Fundamentals and Applications* (John Wiley & Sons, Inc., USA) (2001).
67. P. Parpot, K. B. Kokoh, B. Beden, and C. Lamy, *Electrochim. Acta*, **38**, 1679 (1993).
68. E. Gileadi, *Electrodes Kinetics for Chemists, Chemical Engineers, and Materials Scientists* (John Wiley & Sons, VCH, New York, N Y, USA) (1993).
69. A. Koca, *Electrochem. Commun.*, **11**, 838 (2009).
70. A. Koca, M. K. Şener, M. B. Koçak, and A. Gül, *Trans. Met. Chem.*, **30**, 399 (2005).
71. M. Stojičkov et al., *Eur. J. Inorg. Chem.*, **2020**, 3347 (2020).
72. Z. Huang, P. Zhang, X. Gao, D. Henkensmeier, S. Passerini, and R. Chen, *ACS Appl. Energy Mater.*, **2**, 3773 (2019).